Dispersion of the electro-optic properties of cerium-doped $Sr_{0.61}Ba_{0.39}Nb_2O_6$

Mirco Imlau,[a] Kathrin Bastwöste, Stefan Möller, and Uwe Voelker
Department of Physics, University of Osnabrück, Barbarastrasse 7, D-49069 Osnabrück, Germany

Mikhail Goulkov
Institute of Physics, National Academy of Sciences of Ukraine, Science Avenue 46, 03650 Kiev, Ukraine

(Received 10 April 2006; accepted 19 June 2006; published online 15 September 2006)

The product of the linear electro-optic coefficient with the electron-hole competition factor $r_{33}\zeta$ is determined as a function of the wavelength together with the photorefractive trap density N_{eff} in cerium-doped strontium barium niobate. The photorefractive method of photoinduced light scattering is applied. A pronounced increase of r_{33} by more than a factor of 2 is self-evident in the blue-green spectral range, which is described by a theoretical approach based on the combination of the Sellmeier formulation and the polarization tensor concept. By this further important material parameters are estimated, such as the strength and frequency of the average dipole oscillator characterizing the optical interband transfer. © *2006 American Institute of Physics*.
[DOI: 10.1063/1.2338596]

I. INTRODUCTION

The electro-optic properties are very pronounced in the relaxor ferroelectric strontium barium niobate[1] ($Sr_{0.61}Ba_{0.39}Nb_2O_6$, SBN) and bring about much attention to use SBN for applications in different fields of nonlinear optics. The particular impact of the linear electro-optic effect is attached to photorefraction[2] as it transfers an optically induced spatial charge distribution into a modulation of the index of refraction. It results in the recording of highly efficient volume phase gratings in SBN. The electro-optic properties, and hence the photorefractive response of SBN, can be selectively influenced by doping with different elements,[3,4] which is an important advantage for the development of applications such as holographic data storage.[5] In addition crystals of SBN ensure a high optical quality and can be grown with high purity in the congruently melting composition.[6] In order to assist the progress in photorefractive applications, a broadened knowledge, in particular, about the electro-optic and photorefractive properties of doped SBN is required.

The largest electro-optic coefficient r_{33} usually is determined with interferometric methods.[7] Photorefractive methods based on two-beam coupling[8,9] or photoinduced light scattering[10] were introduced using SBN as an example. The photorefractive methods are advantageous as they allow us to determine simultaneously additional material parameters such as the photorefractive trap density N_{eff}. It is even possible to measure all electro-optic coefficients with only one crystal cut.[11] It was shown that the scattering method especially is simple and requires marginal experimental effort.[10]

The proper design and optimization of optical devices based on photorefractive crystals of SBN require the knowledge of the dispersive behavior of the photorefractive—especially of the electro-optic—properties, which is not reported in literature up to now. In this article we apply the photoinduced light scattering method to determine the linear electro-optic coefficient r_{33} in the spectral range $\lambda = 450-650$ nm. We found a strong increase of r_{33} with decreasing wavelengths, and model the determined dispersive behavior using the combination of the Sellmeier formulation and the polarization tensor concept. In addition the photorefractive trap density N_{eff} is determined which reflects the number densities of traps involved in the photorefractive process.

II. PHOTOREFRACTIVE METHOD

The dispersion of the electro-optic properties of SBN will be determined from the study of the photorefractive phenomenon of photoinduced light scattering. The method is based on the dependence of the photorefractive effect on the linear electro-optic effect, and was recently approved for the determination of the temperature dependence of r_{33} in SBN at $\lambda = 633$ nm.[10] The basic concept of the method is the following.

The scattering appears in SBN crystals upon exposure to a coherent laser beam with a wave vector $\mathbf{k}_p$ orthogonal to the c axis and extraordinary light polarization (see Fig. 1).

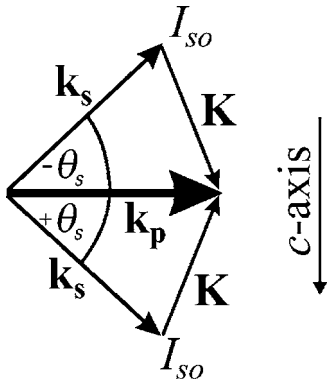

FIG. 1. The beam of a coherent light source with wave vector $\mathbf{k}_p$ propagates through the SBN crystal and is partially scattered from optical inhomogeneities and imperfections in the crystal.

[a]Author to whom correspondence should be addressed; FAX: +49 541 969 3510; electronic mail: mimlau@uos.de; URL: http:\\www.mimlau.de

The pump beam is partially scattered from optical inhomogeneities and imperfections in the crystal.

This initial optical noise consists of seed waves $\mathbf{k}_s$ with intensities I_{so} propagating at angles $+\theta_s$ and $-\theta_s$ with respect to the direction of the pump beam. Interference of seed waves with the pump wave results in the recording of volume phase gratings with wave vector $\mathbf{K}=\mathbf{k}_p-\mathbf{k}_s$ via the photorefractive effect. Photoexcited charge carriers diffuse to the dark regions of the interference pattern and create a space-charge field with a spatial phase shift of $\pi/2$. The electric field yields a spatial modulation of the refractive index via the linear electro-optic effect. A stationary energy exchange by two-wave mixing (2WM) on the recorded grating results in an exponential change of the intensity of the seed waves,

$$I_s(\theta_s) = I_{so}(\theta_s)\exp[(\Gamma(\theta_s) - \alpha)l]. \tag{1}$$

Here, l is the interaction length between the waves, α the absorption coefficient of the medium and the exponential increment,

$$\Gamma(\theta_s) = \frac{q\zeta r_{\text{eff}} n^4 \sin(\theta_s)\cos^2(\theta_s)}{(\lambda^2 q^2/4\pi^2 k_B T) + [4\epsilon_{33}\epsilon_0 n^2 \sin^2(\theta_s/2)]/N_{\text{eff}}} \tag{2}$$

is the gain coefficient for the particular conditions of our experiment describing the efficiency of the direct coupling between the waves $\mathbf{k}_p$ and $\mathbf{k}_s$ at the grating $\mathbf{K}$. Here, $q=-e$ and e is the elementary charge, k_B the Boltzmann constant, T the absolute temperature, ϵ_{33} the component of the relative permittivity of SBN in c direction, and ϵ_0 the permittivity of free space. The factor $|\zeta| \leqslant 1$ is introduced to account for electron-hole competition in the space-charge transport. The effective value of the electro-optic coefficient r_{eff} in c direction is composed by the corresponding largest components of the electro-optic tensor r_{33}, the elasto-optic tensor p_{33}, the piezoelectric stress tensor e_{33}, and the elastic stiffness tensor C_{33},[12]

$$r_{\text{eff}} = r_{33} + \frac{p_{33}e_{33}}{C_{33}}. \tag{3}$$

An estimate of the second summand of Eq. (3) with published data given in Refs. 13–15 yields a modulus of approximately 17 pm/V at $\lambda=632.8$ nm. Values of the electro-optic coefficient for SBN:Ce are comparably large, e.g., $r_{33}=(246\pm12)$ pm/V,[16] so that we approximate $r_{\text{eff}}\approx r_{33}$ with accuracy better than 10%.

Equation (2) has been derived with the following assumptions: (a) predominance of 2WM between the strong pump beam and scattered waves, i.e., negligence of interactions between multiple weak seed waves,[17] which is reasonable according to the results of Ref. 10, (b) an undepleted pump approximation,[9,18] (c) a small absorption coefficient α for the particular investigated wavelengths and $\Gamma > \alpha$, respectively, (d) diffusion of photocarriers as dominating charge transport mechanism,[19] and (e) a major contribution of electrons to photoinduced currents.[8]

We assume equal seed intensities $I_{so}(+\theta_s)=I_{so}(-\theta_s)$. According to Eq. (2) the gain factor for two symmetric scattering angles differs only in its sign $[\Gamma(+\theta_s)=-\Gamma(-\theta_s)]$. This results in an asymmetry of the scattering distribution along the c axis. The scattering intensities $I_s(-\theta_s)$ and $I_s(+\theta_s)$ then yield the gain factor as a function of the scattering angle via

$$|\Gamma(\theta_s)| = \frac{1}{2l}\ln\left[\frac{I_s(-\theta_s)}{I_s(+\theta_s)}\right]. \tag{4}$$

Thus, with Eq. (4), the angular dependence of the gain factor $\Gamma(\theta_s)$ from the angular distribution of the scattered light can be determined. Then, the parameters ζr_{33} and N_{eff} can be obtained according to Eq. (2) by using values of the refractive index n and the effective relative permittivity ϵ_{33}.

The interaction length of scattered and pump waves in Eq. (4) is identified with the crystal thickness $l=d$, i.e., the largest contribution to the initial optical noise is assumed to result from scattering of the incident beam at imperfections of the surface or the bulk region near to the surface. The assumption is valid for the entire investigated angular range of the scattered waves if the diameter of the pump beam d_p is related to the crystal thickness by at least $d_p \geqslant d$.

In order to apply the scattering method for dispersive investigations of $r_{33}\zeta$, all model assumptions should be valid for a broad spectral range. This results, in particular, demands for the experimental conditions as well as for the SBN samples.

III. EXPERIMENTAL SETUP

For our investigations a single crystal of SBN doped with 0.04 mol % cerium was grown by the Czochralski technique from the congruently melting composition and cut into a rectangular parallelepiped with dimensions $a\times b\times c=5\times2\times4$ mm^3. Prior to each measurement the sample was poled by heating it up to 150 °C, applying an external electric field of 350 V/mm$\|c$, and then slowly cooling down to room temperature before removing the field.

A low doping concentration is chosen in order to fit the model requirement of a small absorption coefficient α. In SBN:Ce α depends in the blue-green spectral range on the strength of the Ce-absorption band and is influenced by the tail of the band gap absorption. This could result in different scattering properties for the blue-green, red, and infrared spectral ranges due to absorption processes if the content of Ce is high. Also, a small α allows us to avoid the effect of local optical heating of the samples by the incident light, that also could change the material parameters of the crystal and therewith the scattering.[20]

Figure 2 shows the absorption spectrum of the crystal for extraordinarily polarized probing light $\alpha_e(\lambda)$. The broad absorption band centered at about 500 nm is attributed to cerium.[19]

The values of α_e and of the gain factor Γ are compared in the inserted table for three typical wavelengths. The Γ values are determined from standard two-beam coupling experiments (see e.g., Ref. 11) with the following experimental conditions: extraordinary light polarization of the recording beams, internal Bragg angle $2\theta_B=5.2°$, and modulation depth $m=0.1$. An experimental error of 10% can be estimated for Γ. Obviously, the sample fulfills the important condition $\Gamma > \alpha_e$ in this recording geometry within the entire investigated spectral range.

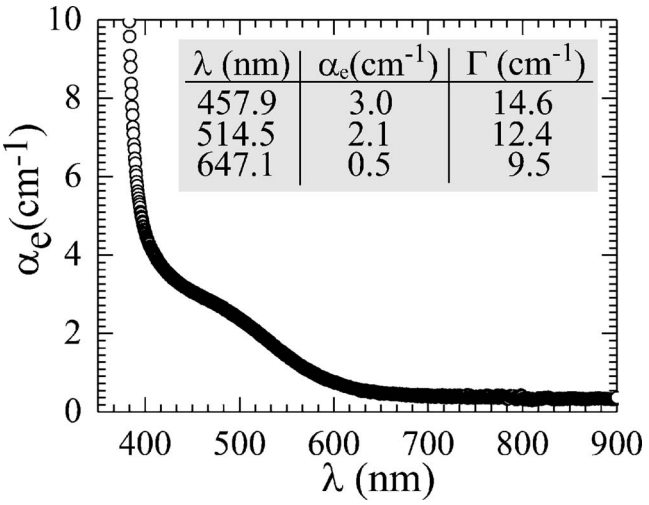

FIG. 2. Dispersion of the extraordinary absorption coefficient $\alpha_e(\lambda)$ of SBN doped with 0.04 mol % cerium. The data set is corrected for reflection losses. The residual absorption in the infrared spectral range is attributed to the surface properties of the sample. The values of the absorption coefficient α_e and the gain factor Γ are compared in the inserted tabular for three distinct wavelengths used in the experiment.

A small thickness of the sample allows us to keep the maximum coupling strength $\Gamma l \leqslant 3$ and, therefore, to avoid a significant pump beam depletion in the entire used spectral interval as suggested by the model. A further reduction of Γl is not useful as it can limit the possibility to determine the intensity of the scattered light with sufficient signal-to-noise ratio.

A sketch of the experimental setup is shown in Fig. 3. An argon-krypton-ion laser is used as coherent light source covering a broad wavelength range from 457.9 up to 647.1 nm. The laser beam serving as pump beam is directed normally to the large *a-c* plane of the sample and can be adjusted in intensity by a combination of a half-wave retarder plate and a Glan-Thompson prism. Extraordinary light polarization of the pump beam is chosen in all experiments. A photodiode (PD) placed behind the sample at a distance of about 14 cm is mounted on a rotation stage driven by an electronic motion controller. Therewith the intensity distribution of the scattered light is scanned on an exact semicircle

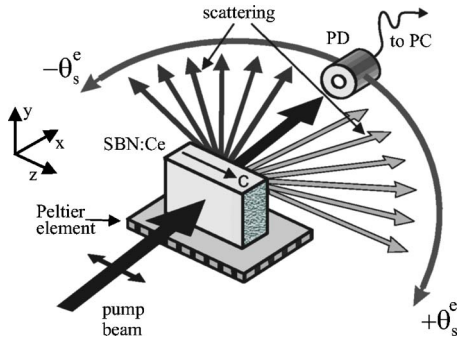

FIG. 3. Experimental setup for measuring the angular distribution of the scattered light at different wavelengths. The beam of an Ar^+-Kr^+ laser impinges normal to the SBN:Ce crystal. The scattered light is detected by the photodiode PD scanning the distribution of the scattered light in an exact semicircle around the sample within the plane of incidence parallel to the *c* axis.

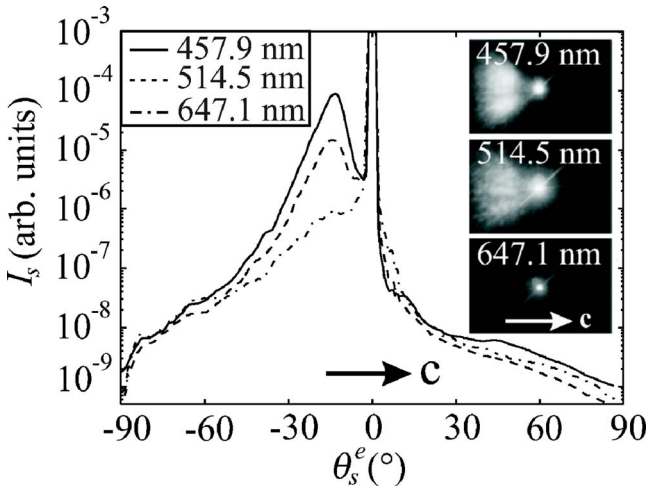

FIG. 4. Angular distribution of the scattered light in SBN for three different wavelengths $\lambda = 457.9$, 514.5, and 647.1 nm with $\mathbf{E} \| c$ and an intensity of $I = 700$ mW/cm^2. The inset shows the corresponding photographs of the scattering pattern taken on a screen behind the crystal.

around the sample along the *c* axis. This allows us to measure the intensities in an angular range of $-90° \leqslant \theta_s^e \leqslant +90°$. Taking the refractive index of SBN for extraordinary light polarization into account this corresponds to an internal angular range of $-26° \leqslant \theta_s \leqslant +26°$. The diameter of the laser beam is $d_p \approx 1.5$ mm, so that $d_p \approx d$ holds. The incoming power of the pump beam is limited to 15 mW for all particular wavelengths in order to avoid thermal effects which may occur by absorption processes. The sample itself is kept at a constant temperature of $T = (40.0 \pm 0.3)$ °C to slightly enhance the gain factor and thus to get a sufficient signal-to-noise ratio of the scattering intensities. All measurements are performed in the steady state.

IV. EXPERIMENTAL RESULTS

Figure 4 displays the one-dimensional angular profile of the steady-state scattering intensity pattern for wavelengths $\lambda = 457.9$, 514.5, and 647.1 nm. Corresponding photographs of the scattering pattern are given in the inset. Obviously, the angular distribution of the scattered light is asymmetric aside the directly transmitted laser beam at $\theta_s = 0°$ in accordance with Eq. (1): in the negative angular range, i.e., in the $-c$ direction, there is a pronounced scattering intensity distribution with a broad maximum at $\theta_s^{e,\max} = 13.5°$. In contrast, at positive scattering angles the scattering intensity is four orders of magnitude weaker. It is remarkable that the intensity of the scattered light increases with decreasing wavelength while at the same time the shape of the scattering distribution becomes more and more pronounced. Similar distributions were determined for all available wavelengths. The photographs allow us to analyze qualitatively the intensity distribution of the scattering lobes also in a direction orthogonal to the polar *c* axis. By this we note a characteristic but not very pronounced lobe structure at all wavelengths of the pump beam.

From the measured angular intensity distributions of the scattered light we extracted the gain factor as a function of the scattering angle via Eq. (4). Figure 5 shows $\Gamma(\theta_s)$ for the

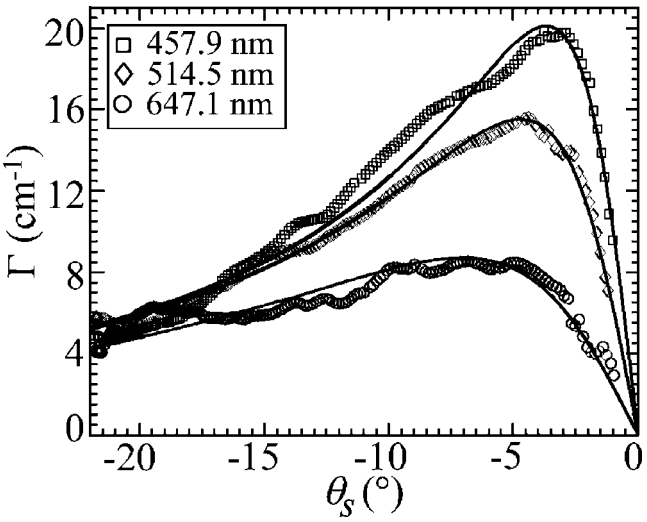

FIG. 5. Absolute value of the two-beam coupling gain Γ vs the internal scattering angle θ_s for three different wavelengths. The thin solid lines are fits with Eq. (2).

three wavelengths determined from the experimental data of Fig. 4. The gain factor Γ shows a characteristic broad angular dependence—in accordance with the photorefractive model for two-wave mixing—with a maximum value of 8 cm^{-1} at λ=647.1 nm up to 20 cm^{-1} at λ=457.9 nm. The lines correspond to fits with Eq. (2) with the refractive index for extraordinarily polarized light of the particular wavelength[21] and dielectric permittivity.[15] The fits result from an iterative fitting procedure to the experimental data set $\Gamma(\theta,\lambda)$ with the independent parameters ζr_{33} and N_{eff}. The latter was set to be wavelength independent in accordance with the assumptions of our model. The procedure succeeded with an average value of $N_{\text{eff}}=(6\pm2)\times10^{21}$ m^{-3} and the dependency $\zeta r_{33}(\lambda)$ is shown in Fig. 6.

V. DISCUSSION

A. Determination of the electro-optic properties

The experimental results show that photoinduced light scattering appears upon exposure to coherent laser light in a

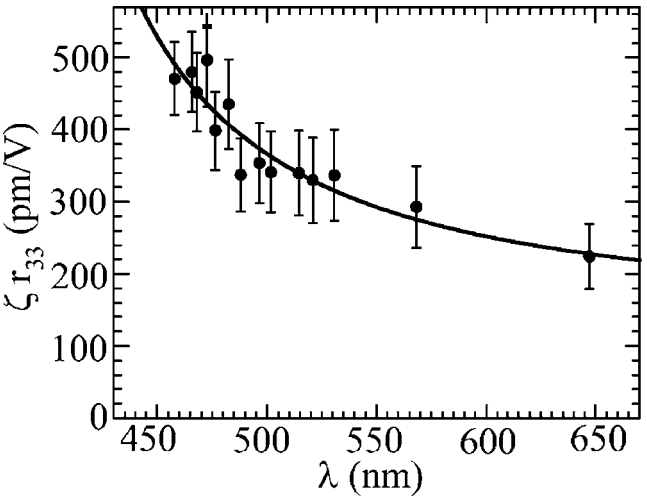

FIG. 6. Wavelength dependence of the product of the electron-hole competition factor and the electro-optic coefficient ζr_{33}. Experimental data (filled circles) and fit according to Eq. (7) (straight line).

TABLE I. Comparison of the data of different SBN samples at room temperature for the wavelength λ=632.8 nm from interferometric and photorefractive methods. In case of photorefractive methods the product ζr_{33} is given. Note that the data of this article refer to the wavelength λ =647.1 nm.

Ce concentration (mol %)	r_{33} (pm/V)[a]	ζr_{33} (pm/V)[b]	Reference
0.04		224±22	This article
0.66		333±23	11
0.66		324±16	10
0.66	354±2		22
0.04	246±12		16
Undoped	235±20		1
Undoped	237±3		7

[a]From interferometric method.
[b]From photorefractive method.

broad spectral range from 457.9 to 647.1 nm and can be used to determine the dispersive behavior of the electro-optic properties of SBN. The applicability and validity of the photorefractive-scattering method for the determination of r_{33} and N_{eff} as well its comparison with standard interferometric methods are discussed in detail in Ref. 10 for SBN doped with 0.66 mol % Ce and for the pump-beam wavelength λ=632.8 nm.

The increase of the intensity of the scattering in the blue-green spectral range observable in Fig. 4 obviously is a result of the increase of the gain factor Γ to smaller wavelengths (see Figs. 2 and 5). Therewith the relation $\Gamma(\lambda)>\alpha(\lambda)$ holds in the entire interval of scattering angles. The experimental error for the determination of Γ by photoinduced light scattering strongly depends on the signal-to-noise ratio of the measured intensities especially of the depleted initially scattered waves in $+\theta_s$ direction.

The accuracy for the determination of the electro-optic coefficient and effective trap density depends on the quality of the fitting procedure. Here, ζr_{33} influences only the absolute value of Γ, while N_{eff} defines also the angular position of the maximum of $\Gamma(\theta_s)$. Obviously, the absolute of Γ shows a pronounced dependence on the wavelength and can be determined well in the entire investigated spectral range. The angular position of the maximum of $\Gamma(\theta_s)$ varies only slightly and can be determined with comparably low accuracy, in particular, in the red spectral range. Taking the experimental error for Γ into account we thus estimate an upper limit of the error of about 10% for the determination of ζr_{33} at λ =475.9 nm and of 20% at λ=647.1 nm. The error for the determination of the photorefractive trap density is at least 30%.

In Table I, the values of the linear electro-optic coefficient in the red spectral range are compared with literature data determined as well from interferometric as from two-beam coupling methods for the wavelength λ=632.8 nm. For reasons of comparability the presented data set for the Ce-doped samples refers to investigations of SBN crystals entirely grown by Dr. R. Pankrath.

It is obvious that the product ζr_{33} derived from our investigations is in agreement with literature data for the linear

electro-optic coefficient of undoped SBN determined with interferometric methods.[1,7] Our value is slightly smaller compared with the value of the SBN sample with the same doping concentration[16] which can be related to the contribution of the electron-hole competition factor. By comparison we get $\zeta \approx 0.91$ in accordance with $\zeta \approx 0.92$ reported in Ref. 10 for $\lambda = 632.8$ nm and a doping concentration of 0.66 mol % Ce.

The difference might also be attributed to the piezoelectric and elasto-optic contributions according to Eq. (3) not considered in our analysis. Following this approach and according to our estimate, we could correct the determined value of the electro-optic coefficient by 17 pm/V, which is indeed in the range of our experimental error. This contribution should be taken into account together with the rotational part of the elasto-optic tensor in order to explain the two-dimensional lobe structure of the scattering in detail, i.e., the intensity distribution in the direction orthogonal to the *c* axis. It can be expected that this accounts for the appearing slight fine structure in the scattering pattern (see photographs of Fig. 4) like it was shown for the characteristic and very pronounced scattering lobes in photorefractive crystals of $BaTiO_3$.[23]

The determined photorefractive trap density in the order of 10^{21} m^{-3} is found in good agreement with literature values.[8,9] Cerium is identified as deep photorefractive center in SBN,[24] so that the photorefractive trap density N_{eff} can be suggested as[25]

$$N_{\mathrm{eff}} = \frac{\tilde{n}(\mathrm{Ce}^{3+}) \cdot \tilde{n}(\mathrm{Ce}^{4+})}{\tilde{n}(\mathrm{Ce}^{3+}) + \tilde{n}(\mathrm{Ce}^{4+})}, \tag{5}$$

where $\tilde{n}(\mathrm{Ce}^{3+})$ and $\tilde{n}(\mathrm{Ce}^{4+})$ are the number densities of cerium in the valence states 3+ (donor) and 4+ (acceptor) effectively contributing to the photoelectric formation of the space-charge field. It should be noted that our value is about three orders of magnitude lower compared with the total number density $N = n(\mathrm{Ce}^{3+}) + n(\mathrm{Ce}^{4+}) = 3.3 \times 10^{24}$ m^{-3} estimated from neutron activation analysis of Ce-doped SBN crystals[6] with the particular cerium content of 0.04 mol %. This result reflects the significant difference between effectively involved number densities of traps $\tilde{n}(\mathrm{Ce}^{3+,4+})$ and the trap number densities $n(\mathrm{Ce}^{3+,4+})$ as already discussed in Ref. 26. The difference is attributed to the fact that only a fraction of the available traps, i.e., about 0.1%, participates to the photoelectric process in the investigated SBN sample. Here, the photon cross section of the Ce^{3+} ions and the effective trapping cross section of the Ce^{4+} ions have to be considered.[27]

B. Dispersive behavior of ζr_{33}

The dispersive behavior of ζr_{33} is very remarkable due to the increase by more than a factor of 2 in the blue-green spectral range and can result from the wavelength dependence of $\zeta(\lambda)$ and/or by $r_{33}(\lambda)$. A dispersive behavior of ζ may occur, if different kinds of photocarriers, e.g., electrons and holes, are involved in the process of the electric charge transport.[28] However, electrons usually are assumed as dominating contributors to the photoinduced current in SBN,[8] i.e., at least $0 < \zeta \leq 1$. Up to now there is only one reliable experimentally determined value of $\zeta \approx 0.92$ estimated at $\lambda = 632.8$ nm.[10] Taking this value and $\zeta_{\max} = 1$ into account, the product ζr_{33} obviously can not be increased by more than about 10% in the blue spectral range solely by the electron-hole competition factor. Considering a decrease of ζ with decreasing wavelength, the principle dispersive behavior of $r_{33}(\lambda)$ will not be affected besides its maximum values. Hence, in any case the observed dispersion of ζr_{33} uncovers a pronounced dispersion of $r_{33}(\lambda)$.

The increase of *r* with decreasing wavelength is a property already reported in other ferroelectric oxidic crystals. In Fe-doped $LiNbO_3$ single crystals r_{33} increases by 16% in the range from 632.8 to 457.9 nm (Table I and Fig. 2 in Ref. 29). The experimentally determined electro-optic coefficients of $BaTiO_3$ show an increase of up to approximately 38% (Fig. 5 in Ref. 30).

To discuss the origin of the pronounced dispersion of $r_{33}(\lambda)$ in SBN:Ce we assume $\zeta = 1$ and we have to point to the dispersive behavior of the quadratic electro-optic coefficient $g_{33}(\lambda)$ due to the relation

$$r_{33}(\lambda) = 2\epsilon_0 \epsilon_{33} g_{33}(\lambda) P_s, \tag{6}$$

which holds for the point group symmetry 4 mm of SBN.[31] Here, P_s is the spontaneous polarization along the *c* axis and we neglect a wavelength dependence of ϵ_{33} within the investigated spectral range. An expression for the dispersion of $g_{33}(\lambda)$ is derived in Ref. 32 by combining the wavelength derivative of a Sellmeier equation and the polarization potential tensor concept for tetragonal ferroelectrics.[33] Introducing $g_{33}(\lambda)$ in Eq. (6) we find

$$r_{33}(\lambda) = \frac{\epsilon \epsilon_0 P_s f_e \beta}{2\pi^3 \hbar c^3 n^4(\lambda) \lambda_e [(1/\lambda_e^2) - (1/\lambda^2)]^2}, \tag{7}$$

where $\hbar$ is the reduced Planck constant, *c* is the light velocity, and β is the effective coefficient of the polarization potential tensor for $\mathbf{E} \| c$ axis according to the polarization potential tensor concept.[34] Furthermore, ω_e is the average oscillator frequency, $\lambda_e = 2\pi c/\omega_e$ the corresponding wavelength, and f_e is the average oscillator strength in the applied Sellmeier formulation. Following this approach we note that the optical properties at long wavelengths are assumed to be determined predominantly by the particular dipole oscillator of *lowest* energy. Summing the contributions of all dipole oscillators, the resulting single-term Sellmeier relation was shown to be characterized by ω_e and f_e. Both parameters are connected with the energy-band structure of SBN defined by the $2p$ orbitals of the oxygen atoms (valence band) and the *d* orbital of the central Nb atom in the NbO_6 octahedron (lowest-lying empty conduction band). Hence ω_e and f_e characterize the optical interband transfer and are additional important material parameters which can be determined with our analysis.

The fit of Eq. (7) to the experimental data with the free parameters $A = \epsilon_0 \epsilon_{33} P_s f_e \beta / (2\pi^3 \hbar c^3)$ and λ_e yields $A = (8 \pm 4) \times 10^{10}$ m^{-2} V^{-1} and $\lambda_e = (338 \pm 24)$ nm. The corresponding function is plotted as solid line in Fig. 6 and obviously describes our experimental data and the observed dispersion very well. From the parameter *A* together with

typical values of the spontaneous polarization $P_s = 25\ \mu C/cm^2$ (Ref. 35) and the polarization potential $\beta = 3.4\ eV\ m^4/C^2$ (Ref. 32) we estimate the dipole strength $f_e = (2 \pm 0.5) \times 10^{31}\ s^{-2}$. Although there are no literature values available for SBN:Ce, the obtained value agrees fairly well with $f_e \approx 10^{32}\ s^{-2}$ of other oxide crystals.[36] The wavelength λ_e gives an estimate for the energy of the dipole oscillator of lowest energy, i.e., the energy of the optical interband transfer: $E_e = (3.7 \pm 0.26)$ eV. For comparison, the band edge energy of SBN at 40 °C determined from absorption spectroscopy is $E_g \approx 3.4$ eV.[37]

VI. SUMMARY AND CONCLUSION

The dispersive behavior of the photorefractive properties of cerium-doped SBN, in particular of the product of the linear electro-optic coefficient with the electron-hole competition factor $(r_{33}\zeta)(\lambda)$, has been determined with the method of photoinduced light scattering. We can reasonably model the increase of the linear electro-optic effect by more than a factor of 2 in the blue-green spectral using a theoretical approach by combining the Sellmeier formulation with the polarization tensor concept. We further determined important material parameters from the analysis of photoinduced light scattering such as the strength and frequency of the average dipole oscillator characterizing the optical interband transfer.

ACKNOWLEDGMENTS

Financial support from the Deutsche Forschungsgemeinschaft within the Graduiertenkolleg GRK 695 and project IM 37/2-2 is gratefully acknowledged. The authors like to thank Professor Dr. M. Wöhlecke for fruitful discussion and Dr. R. Pankrath for supplying the samples.

[1] S. Ducharme, J. Feinberg, and R. R. Neurgaonkar, IEEE J. Quantum Electron. **QE-23**, 2116 (1987).
[2] *Photorefractive Materials and Their Applications II*, Topics in Applied Physics Vol. 62, edited by P. Günter and J.-P. Huignard (Springer, Berlin, 1989).
[3] K. Buse, Appl. Phys. B: Lasers Opt. **B64**, 391 (1997).
[4] T. Woike, U. Dörfler, L. Tsankov, G. Weckwerth, D. Wolf, M. Wöhlecke, T. Granzow, R. Pankrath, M. Imlau, and W. Kleemann, Appl. Phys. B: Lasers Opt. **B72**, 661 (2001).
[5] J. E. Ford, J. Ma, and Y. Fainman, J. Opt. Soc. Am. A **9**, 1183 (1992).
[6] Th. Woike, G. Weckwerth, H. Palme, and R. Pankrath, Solid State Commun. **102**, 1674 (1998).
[7] H. Y. Zhang, X. H. He, Y. H. Shih, and S. H. Tang, Opt. Commun. **86**, 509 (1991).
[8] M. D. Ewbank, R. R. Neurgaonkar, W. K. Cory, and J. Feinberg, J. Appl. Phys. **62**, 374 (1987).
[9] R. A. Vazquez, F. R. Vachss, R. R. Neurgaonkar, and M. D. Ewbank, J. Opt. Soc. Am. B **8**, 1932 (1991).
[10] M. Goulkov, T. Granzow, U. Dörfler, Th. Woike, M. Imlau, R. Pankrath, and W. Kleemann, Opt. Commun. **218**, 173 (2003).
[11] U. B. Dörfler *et al.*, Appl. Phys. B: Lasers Opt. **B68**, 843 (1999).
[12] P. Günter and M. Zgonik, Opt. Lett. **16**, 1826 (1991).
[13] N. M. Shorrocks, R. W. Whatmore, and S. T. Liu, J. Phys. D **15**, 2469 (1982).
[14] E. L. Venturini, E. G. Spencer, and A. A. Ballman, J. Appl. Phys. **40**, 1622 (1969).
[15] R. R. Neurgaonkar and L. E. Cross, Mater. Res. Bull. **21**, 893 (1986).
[16] M. Wesner, C. Herden, D. Kip, E. Krätzig, and P. Moretti, Opt. Commun. **188**, 69 (2001).
[17] M. Segev, Y. Ophir, and B. Fischer, Opt. Commun. **77**, 265 (1990).
[18] N. V. Kukhtarev, V. P. Markov, S. G. Odulov, M. S. Soskin, and V. L. Vinetskiĭ, Ferroelectrics **22**, 961 (1979).
[19] K. Buse, U. van Stevendaal, R. Pankrath, and E. Krätzig, J. Opt. Soc. Am. B **13**, 1461 (1996).
[20] M. Goulkov, O. Fedorenko, Th. Woike, T. Granzow, M. Imlau, and M. Wöhlecke, J. Phys.: Condens. Matter **18**, 3037 (2006).
[21] Th. Woike, T. Granzow, U. Dörfler, C. Poetsch, M. Wöhlecke, and R. Pankrath, Phys. Status Solidi A **186**, R13 (2001).
[22] V. Wirth, Ph.D. thesis, Köln University, 1999.
[23] G. Montemezzani, A. A. Zozulya, L. Czaia, D. Z. Anderson, M. Zgonik, and P. Günther, Phys. Rev. A **52**, 1791 (1995).
[24] R. Niemann, K. Buse, R. Pankrath, and M. Neumann, Solid State Commun. **98**, 209 (1996).
[25] K. Buse, Appl. Phys. B: Lasers Opt. **B64**, 273 (1997).
[26] D. Schaniel, Th. Woike, G. Weckwerth, J. Schefer, M. Imlau, M. Wöhlecke, and R. Pankrath, Phys. Rev. B **70**, 144410 (2004).
[27] K. Buse, A. Gerwens, S. Wevering, and E. Krätzig, J. Opt. Soc. Am. B **15**, 1674 (1998).
[28] R. Orlowski and E. Krätzig, Solid State Commun. **27**, 1351 (1978).
[29] S. Fries and S. Bauschulte, Phys. Status Solidi A **125**, 369 (1991).
[30] A. R. Johnston, J. Appl. Phys. **42**, 3501 (1971).
[31] A. J. Fox, J. Appl. Phys. **44**, 254 (1973).
[32] M. E. Lines and A. M. Glass, *Principles and Applications of Ferroelectrics and Related Materials* (Clarendon, Oxford, 1977).
[33] M. DiDomenico and S. H. Wemple, J. Appl. Phys. **40**, 720 (1969).
[34] J. D. Zook and T. N. Casselman, Phys. Rev. Lett. **17**, 960 (1966).
[35] S. H. Wemple and M. DiDomenico, J. Appl. Phys. **40**, 735 (1969).
[36] W. L. Bond, J. Appl. Phys. **36**, 1674 (1965).
[37] M. Meyer, M. Wöhlecke, and O. F. Schirmer, Phys. Status Solidi B **221**, R1 (2000).